Optimizing entangling quantum gates for physical systems

M. M. Müller,[1] D. M. Reich,[2, 3] M. Murphy,[1] H. Yuan,[4] J. Vala,[5, 6] K. B. Whaley,[7] T. Calarco,[1] and C. P. Koch[2, 3]

[1]*Institut für Quanteninformationsverarbeitung, Universität Ulm, 89081 Ulm, Germany*
[2]*Institut für Theoretische Physik, Freie Universität Berlin, Arnimallee 14, 14195 Berlin, Germany*
[3]*Institut für Physik, Universität Kassel, Heinrich-Plett-Str. 40, 34132 Kassel, Germany*
[4]*Research Laboratory of Electronics, Massachusetts Institute of Technology, Cambridge, MA 02139*
[5]*Department of Mathematical Physics, National University of Ireland, Maynooth, Ireland*
[6]*School of Theoretical Physics, Dublin Institute for Advanced Studies, 10 Burlington Rd., Dublin, Ireland*
[7]*Department of Chemistry, University of California, Berkeley, California 94720, USA*
(Dated: January 19, 2013)

Optimal control theory is a versatile tool that presents a route to significantly improving figures of merit for quantum information tasks. We combine it here with the geometric theory for local equivalence classes of two-qubit operations to derive an optimization algorithm that determines the best entangling two-qubit gate for a given physical setting. We demonstrate the power of this approach for trapped polar molecules and neutral atoms.

I. INTRODUCTION

Quantum information science requires extreme accuracy in implementation of quantum tasks such as gate operations, in order to fulfill the stringent criteria of fault tolerance [1]. However the dynamics underlying a gate operation is often very complex, occurring in a Hilbert space much larger than that of the qubits. Optimal quantum control then provides an indispensable tool for obtaining a high-fidelity implementation [2]. Realization of a universal set of gates comprises multiple levels of difficulty, because different physics is typically involved for one- and two-qubit operations. For many qubit systems, two-qubit gates are the most challenging since they involve controlled interaction between two otherwise isolated quantum systems. Furthermore, for a given physical implementation, it is not necessarily *a priori* clear which two-qubit gate can best be implemented when the practical criteria of optimal achievable fidelity and realistic gate operation time are imposed.

We address this problem here by combining optimal control theory [2] with the geometric theory for local equivalence classes of two-qubit operations [3].This allows us to develop an algorithm that optimizes for the non-local content of a two-qubit gate rather than for fidelity of a specific gate such as CNOT. The resulting separation of non-local from local control objectives relaxes the control constraints and enables both maximum fidelities to be reached and fundamental limits for control to be identified. We apply our algorithm to trapped polar molecules and neutral atoms, both candidates for realizing quantum computation. Manipulation of trapped polar molecules with microwave fields has been shown to allow realization of effective spin-spin models [4] with continuously tunable parameters. In our first example we use the combined optimal/geometric control algorithm to determine which non-local gates can be realized for a given underlying molecule-microwave field Hamiltonian. In our second example, we obtain optimal solutions for a Rydberg gate [5] between trapped neutral atoms in the presence of both decay processes and entangling couplings between internal and external degrees of freedom. We show that high fidelity Rydberg gate operation is possible even for a configuration where the blockade regime is not reached and despite spontaneous emission from intermediate states.

II. OPTIMIZING THE NON-LOCAL CONTENT OF A TWO-QUBIT GATE

A. Optimal control theory

High-fidelity implementations of quantum gates can be obtained with optimal control theory by defining a suitable distance measure between the desired unitary $\hat{\mathbf{O}}$ and the actual evolution, e.g.,

$$J_T^D = 1 - \frac{1}{N}\mathfrak{Re}\left[\,\mathsf{Tr}\left\{\hat{\mathbf{O}}^+\hat{\mathbf{P}}_N\hat{\mathbf{U}}(T,0;\varepsilon)\hat{\mathbf{P}}_N\right\}\right]\,, \qquad (1)$$

and minimizing it with respect to some external field $\varepsilon(t)$ [2]. Here, $\hat{\mathbf{U}}(T,0;\varepsilon)$ represents the evolution of the system under the action of an external field from time 0 to time T. For example, $\varepsilon(t)$ can be a pulsed laser field or a time-dependent magnetic field. The Hilbert space in which the system evolves is possibly very large. The logical subspace, i.e., the subspace of the total Hilbert space in which $\hat{\mathbf{O}}$ acts has dimension N, $N = \dim\mathcal{H}_O$ ($N = 4$ for a two-qubit gate). $\hat{\mathbf{P}}_N$ denotes the projector onto this subspace. The trace is evaluated by choosing a suitable orthonormal basis of the subspace $\mathcal{H}_O$, $\{|\varphi_{k=1,\dots,N}\rangle\}$. The evolution of the system is thus expressed in terms of the time evolved basis states, $|\varphi_k(T)\rangle = \hat{\mathbf{U}}(T,0;\varepsilon)|\varphi_k\rangle$, and J_T^D becomes a functional of the states $|\varphi_k(T)\rangle$. For the specific choice of Eq. (1), J_T^D is a phase sensitive functional that depends linearly on the states, $|\varphi_k(T)\rangle$, and equals zero for perfect implementations of $\hat{\mathbf{U}}$.

Additional constraints can be introduced to ensure finite pulse fluence,

$$g_a = \lambda_a \int_0^T \left[\varepsilon(t) - \varepsilon_{ref}(t)\right]^2 / S(t) dt\,, \qquad (2)$$

or avoid population of states subject to loss,

$$g_b = \frac{\lambda_b}{NT} \int_0^T \sum_{m=1}^N \langle \varphi_m(t) | \hat{\mathbf{P}}_{avoid} | \varphi_m(t) \rangle dt\,. \qquad (3)$$

Here, $\varepsilon_{ref}(t)$ denotes a reference field, $S(t)$ is a shape function to switch the field smoothly on and off, and λ_a and λ_b are weights [20]. $\hat{\mathbf{P}}_{avoid}$ denotes the projector onto the subspace of the total Hilbert space that shall never be populated, and g_b minimizes population of this subspace [6]. The total functional to be minimized, J, is given by the sum of J_T^D, g_a and g_b,

$$J = J_T^D + g_a + g_b\,. \qquad (4)$$

Solving Eq. (4) with an iterative procedure in which the reference field, $\varepsilon_{ref}(t)$, is chosen at each level of iteration to be the optimized field from the previous iteration ensures vanishing of g_a at the optimum, since this is reached when the optimal value of J is determined only by J_T^D and possibly g_b, but not by the pulse fluence [2]. A monotonically convergent algorithm is obtained for this control problem using a simplified version of Krotov's method [2, 6].

The core idea of Krotov's method [7, 8] consists in disentangling the interdependence of the states and the field. This is achieved by separating the final-time and intermediate-time dependencies of the total functional J and adding to this a vanishing quantity, $\Phi_T - \Phi_0 - \int_0^T \dot{\Phi} dt$, which is expressed in terms of a functional Φ that depends only on the states and not on the field. The freedom of choice in Φ is utilized to ensure monotonic convergence of the algorithm. Specifically, expanding Φ up to second order in the states, $\{\varphi_k(t)\}$, the expansion coefficients are chosen such that the first and second order derivatives of J with respect to the states fulfill the conditions for the extremum and maximum of J, respectively, when J is minimized. Since J thus takes the worst possible value with respect to the choice of basis states, any change of J due to varying the field, $\varepsilon(t)$, then leads to improvement toward the actual target, minimization of J.

For the simple functional of Eq. (4), it turns out that the second order conditions are trivially fulfilled by correct choice of the sign of the weights λ_a and λ_b, and the second order expansion coefficients of Φ can be set to zero [2]. The ensuing algorithm thus coincides with that obtained from straightforward variation of J with a specific discretization of the coupled control equations [9, 10]. It yields pulses that implement the desired gate with high fidelity, provided that the dynamics allow for it [11]. For functionals with higher than quadratic dependence on

the states, however, it is essential to include the second order contribution to Φ in order to ensure monotonic convergence. The second order expansion coefficient can be estimated either analytically or numerically, as detailed in Ref. [12].

B. Geometric theory of non-local two-qubit operations

The group of all two-qubit gates, $SU(4)$, consists of local operations, $SU(2) \otimes SU(2)$, and non-local operations, $SU(4) \backslash SU(2) \otimes SU(2)$. This is a direct result of the existence of a Cartan decomposition of the corresponding Lie algebra [13]. Any two-qubit operation can be written as

$$\hat{\mathbf{U}} = \hat{\mathbf{k}}_1 \hat{\mathbf{A}} \hat{\mathbf{k}}_2 \qquad (5)$$

where

$$\hat{\mathbf{A}} = \exp \left[-\frac{i}{2} \sum_{j=x,y,z} c_j \hat{\boldsymbol{\sigma}}_\mathbf{j} \otimes \hat{\boldsymbol{\sigma}}_\mathbf{j} \right] \qquad (6)$$

and the $\hat{\mathbf{k}}_n \in SU(2) \otimes SU(2)$ are local operators. The set $SU(4) \backslash SU(2) \otimes SU(2)$ is generated by the maximal Abelian subalgebra of the $su(4)$ algebra which is spanned by the operators $\hat{\boldsymbol{\sigma}}_\mathbf{j} \otimes \hat{\boldsymbol{\sigma}}_\mathbf{j}$, $j = x, y, z$. Since these two-qubit operators commute, the operations belonging to $SU(4) \backslash SU(2) \otimes SU(2)$ can be represented by three real numbers (c_x, c_y, c_z). Due to the periodicity of the complex exponential, the c_j take their value from a three-dimensional cube $\mathbf{I}^3$ with edges $\mathbf{I} = [0, \pi]$. The operations from this set create and change entanglement between two qubits (with the exception of the identity operation $\mathbb{1}$ and the SWAP gate for which all $c_j = 0$ mod π and all $c_j = \pi/2$, respectively). Each local operation $\hat{\mathbf{k}}_{1/2} \in SU(2) \otimes SU(2)$ accounts for additional 6 parameters, yielding the remaining 12 parameters that are required to fully characterize the elements of $SU(4)$.

The representation of the non-local content of $\hat{\mathbf{U}}$ in terms of the c_j is not unique. Different points in the cube $\mathbf{I}^3$ may correspond to the same two-qubit operation up to local transformations [3]. For example, all eight corners of the cube are equivalent to the identity operator up to local transformations. This symmetry is characterized by the Weyl reflection group. It is generated by permutations or permutations with sign flips of two entries in (c_x, c_y, c_z). Symmetry reduction of the cube $\mathbf{I}^3$ leads to a geometric representation of non-local two-qubit gates within the Weyl chamber a^+ which is the tetrahedral segment of the cube $\mathbf{I}^3$ spanned by $(c_x, c_y, c_z) = (0, 0, 0)$, $(\pi, 0, 0)$, $(\pi/2, \pi/2, 0)$, and $(\pi/2, \pi/2, \pi/2)$. All two-qubit gates that are equivalent up to local operations $\hat{\mathbf{k}}_n$ are geometrically represented by a single point in the Weyl chamber (except on its base where local equivalence classes may be represented by two symmetry-equivalent
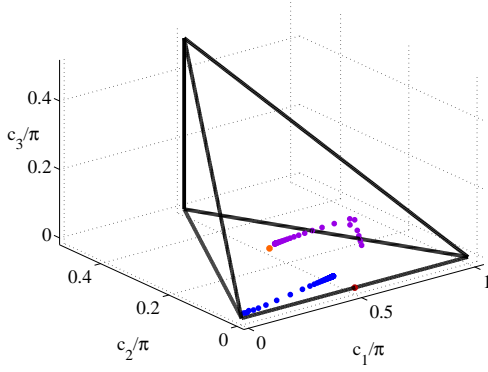
class	c_x	c_y	c_z	g_1	g_2	g_3
[$\mathbb{1}$]	0	0	0	1	0	3
[CNOT]	$\pi/2$	0	0	0	0	1
[CPHASE]	$\pi/2$	0	0	0	0	1
[B-gate]	$\pi/2$	$\pi/4$	0	0	0	0
[$\sqrt{\text{SWAP}}$]	$\pi/4$	$\pi/4$	$\pi/4$	0	1/4	0
[SWAP]	$\pi/2$	$\pi/2$	$\pi/2$	-1	0	-3

TABLE I: Examples of local equivalence classes, their coordinates (c_x, c_y, c_z) in the Weyl chamber, and their local invariants g_1, g_2, g_3

.

FIG. 1: (Color online) Optimization of non-local gates in the Weyl chamber. Local invariants of the B gate (orange) and CNOT (red) are approached iteratively (each violet/blue point corresponds to one step in the optimization of the effective spin-spin Hamiltonian, cf. Section III A below).

points) [3]. For example, CNOT and the controlled π-phase gate (CPHASE) are in the same local equivalence class, which is defined by the point $(\pi/2, 0, 0)$, cf. Fig. 1 (left panel).

Each class of all the two-qubit gates that are equivalent up to local operations, $[\hat{\mathbf{U}}]$, can also be characterized by three real numbers [14], the local invariants g_1, g_2 and g_3.

It was shown in Ref. [3] that there exists a one-to-one correspondence between the points in the Weyl chamber (c_x, c_y, c_z) and the local invariants. For a given unitary $\hat{\mathbf{U}}$, g_1, g_2, g_3 are easily calculated from the representation of $\hat{\mathbf{U}}$ in the Bell basis [3]. Denoting the transformation from the logical basis into the Bell basis by $\hat{\mathbf{Q}}$, $\hat{\mathbf{U}}_B = \hat{\mathbf{Q}}^+ \hat{\mathbf{U}} \hat{\mathbf{Q}} = \hat{\mathbf{o}}_1 \hat{\mathbf{F}} \hat{\mathbf{o}}_2$ where $\hat{\mathbf{o}}_n = \hat{\mathbf{Q}}^+ \hat{\mathbf{k}}_n \hat{\mathbf{Q}} \in SO(4)$ and thus $\hat{\mathbf{o}}_n^T \hat{\mathbf{o}}_n = \hat{\mathbf{o}}_n \hat{\mathbf{o}}_n^T = \mathbb{1}$. The matrix $\hat{\mathbf{F}}$ is diagonal,

$$\hat{\mathbf{F}} = \text{diag}\{e^{\frac{i}{2}(c_x - c_y + c_z)}, e^{\frac{i}{2}(c_x + c_y - c_z)},$$
$$e^{-\frac{i}{2}(c_x + c_y + c_z)}, e^{\frac{i}{2}(-c_x + c_y + c_z)}\}. \quad (7)$$

Introducing a matrix $\hat{\mathbf{m}}_U$,

$$\hat{\mathbf{m}}_U = \hat{\mathbf{U}}_B^T \hat{\mathbf{U}}_B = \hat{\mathbf{o}}_2 \hat{\mathbf{F}}^2 \hat{\mathbf{o}}_2, \quad (8)$$

leads to automatic elimination of the first local factor $\hat{\mathbf{o}}_1$. The local invariants are defined [3] as

$$g_1 = \frac{1}{16} \mathfrak{Re} \, \text{Tr}\{\hat{\mathbf{m}}_U\}^2 \quad (9a)$$
$$= \cos^2 c_x \cos^2 c_y \cos^2 c_z - \sin^2 c_x \sin^2 c_y \sin^2 c_z,$$

$$g_2 = \frac{1}{16} \mathfrak{Im} \, \text{Tr}\{\hat{\mathbf{m}}_U\}^2 \quad (9b)$$
$$= \frac{1}{4} \sin 2c_x \sin 2c_y \sin 2c_z,$$

$$g_3 = \frac{1}{4} \text{Tr}\{\hat{\mathbf{m}}_U\}^2 - \text{Tr}\{\hat{\mathbf{m}}_U^2\} \quad (9c)$$
$$= 4 \cos^2 c_x \cos^2 c_y \cos^2 c_z - 4 \sin^2 c_x \sin^2 c_y \sin^2 c_z$$
$$- \cos 2c_x \cos 2c_y \cos 2c_z,$$

where the remaining local factor $\hat{\mathbf{o}}_2$ is eliminated due to the cyclic permutation invariance of the trace. To generalize the local invariants to the elements of the group $U(4)$, i.e., $\hat{\mathbf{U}} = e^{i\alpha} \hat{\mathbf{U}}' \in U(4)$ where $\hat{\mathbf{U}}' \in SU(4)$, the global phase $e^{i\alpha}$ is eliminated by dividing the local invariants by $\det\{\hat{\mathbf{U}}\} = e^{4i\alpha}$. The final form of the local invariants is then

$$g_1 = \mathfrak{Re} \, \text{Tr}\{\hat{\mathbf{m}}_U\}^2 / 16 \det\{\hat{\mathbf{U}}\}, \quad (10a)$$
$$g_2 = \mathfrak{Im} \, \text{Tr}\{\hat{\mathbf{m}}_U\}^2 / 16 \det\{\hat{\mathbf{U}}\}, \quad (10b)$$
$$g_3 = \text{Tr}\{\hat{\mathbf{m}}_U\}^2 - \text{Tr}\{\hat{\mathbf{m}}_U^2\} / 4 \det\{\hat{\mathbf{U}}\}. \quad (10c)$$

A few examples of local equivalence classes, their coordinates c_i in the Weyl chamber and the corresponding Makhlin invariants g_i are given in Table I.

C. Optimization functional based on the local invariants

To act as a suitable optimization functional, any real-valued functional $J[\{\varphi_k\}]$ should fulfill two necessary conditions: (i) J must strictly take its global optimum for all sets of states $\{\varphi_k\}$ that represent the desired outcome, and (ii) J must be regular, i.e., at least twice differentiable. Moreover, as a matter of practicality, it should be possible to express $J[\{\varphi_k\}]$ explicitly in terms of the states, $\{\varphi_k\}$, in order to carry out the differentiation. While the Weyl chamber coordinates, (c_x, c_y, c_z), are only implicitly given in terms of the evolution $\hat{\mathbf{U}}$ of the system, the local invariants g_1, g_2, g_3 can directly be calculated from $\hat{\mathbf{U}}$ by use of Eqs. (9) (or Eqs. (10) for $\hat{\mathbf{U}} \in U(4)$), and hence from the time-evolved basis states $|\varphi_k(t)\rangle = \hat{\mathbf{U}}|\varphi_k(0)\rangle$. Therefore the local invariants lend themselves naturally to the definition of a distance measure between the desired local equivalence class $[\hat{\mathbf{O}}]$ and the actually realized local equivalence class $[\hat{\mathbf{U}}]$. We define this distance measure as

$$d = \sum_{i=1}^{3} \Delta g_i^2 \quad \text{with} \quad \Delta g_i = |g_i(\hat{\mathbf{O}}) - g_i(\hat{\mathbf{U}}_{T,N})|. \quad (11)$$

The distance d constitutes one component of the desired optimization functional. Since the time evolution of the

physical system typically occurs in a Hilbert space that is much larger than the logical space, $\hat{\mathbf{U}}(T, 0; \varepsilon)$ needs to be projected into the logical subspace,

$$\hat{\mathbf{U}}_{T,N} = \hat{\mathbf{P}}_N \hat{\mathbf{U}}(T, 0; \varepsilon) \hat{\mathbf{P}}_N . \qquad (12)$$

Correspondingly, d needs to be augmented by a term that enforces unitarity in the logical space at the final time T, leading to the following optimization functional for a non-local equivalence class:

$$J_T^{LI} = \Delta g_1^2 + \Delta g_2^2 + \Delta g_3^2 + 1 - \frac{1}{N} \, \text{Tr} \left\{ \hat{\mathbf{U}}_{T,N} \hat{\mathbf{U}}_{T,N}^+ \right\} . \qquad (13)$$

Using the definition of the local invariants, the Δg_i are expressed in terms of the time-evolved basis states as follows. Expanding $\hat{\mathbf{U}}$ in the orthonormal basis $|\varphi_k\rangle$, the

matrix elements of $\hat{\mathbf{m}}_U$ are second order in the states, cf. Eq. (8). Therefore the g_j are fourth order in the states, cf. Eq. (9), and J_T^{LI} turns out to be a polynomial of eighth order in the states. The specific form of J_T^{LI} is given in Appendix A.

For such a non-convex functional, the commonly used optimization algorithms including that of Ref. [2] are not sufficient to ensure monotonic convergence and indeed fail to converge. To the best of our knowledge, Krotov's method is the only approach providing an optimization algorithm that ensures monotonic convergence for arbitrary functionals in quantum control [12]. For difficult control problems, monotonic convergence is essential to reach any optimum, even a local one. Applying Krotov's method to the functional J_T^{LI}, the optimal field is obtained iteratively according to

$$\varepsilon^{(i+1)}(t) = \varepsilon^{(i)}(t) + \frac{S(t)}{\lambda_a} \mathfrak{Im} \left\{ \sum_{k=1}^{N} \left\langle \chi_k^{(i)}(t) \left| \frac{\partial \hat{\mathbf{H}}}{\partial \varepsilon}^{(i+1)} \right| \varphi_k^{(i+1)}(t) \right\rangle + \frac{1}{2} \sigma(t) \sum_{k=1}^{N} \left\langle \Delta \varphi_k^{(i+1)}(t) \left| \frac{\partial \hat{\mathbf{H}}}{\partial \varepsilon}^{(i+1)} \right| \varphi_k^{(i+1)}(t) \right\rangle \right\} , \quad (14)$$

where $|\Delta \varphi_k^{(i+1)}(t)\rangle = |\varphi_k^{(i+1)}(t)\rangle - |\varphi_k^{(i)}(t)\rangle$. The details of the iterative algorithm are presented in Appendix B. In brief, Eq. (14) implies propagating the basis states $|\varphi_k\rangle$ forward in time and the adjoint states $|\chi_k\rangle$ backward in time with the 'initial' condition, $|\chi_k(T)\rangle$, determined by the functional J_T^{LI}. $S(t)/\lambda_a$ and $\sigma(t)$ are parameters of the optimization algorithm that are constructed following the prescription of Ref. [12], cf. Appendix B.

D. Actual gate operation and gate error

Optimizing the functional J_T^{LI} yields some gate $\hat{\mathbf{U}}_{T,N}$ that is, up to some small error, in the local equivalence class of the desired gate $\hat{\mathbf{O}}$. In order to actually implement $\hat{\mathbf{O}}$, we need to determine the local operations $\hat{\mathbf{k}}_1$ and $\hat{\mathbf{k}}_2$ such that $\hat{\mathbf{O}} = \hat{\mathbf{k}}_1 \hat{\mathbf{U}} \hat{\mathbf{k}}_2$. This is achieved by transforming both $\hat{\mathbf{O}}$ and $\hat{\mathbf{U}}_{T,N}$ to the canonical form $\hat{\mathbf{A}}$, $\hat{\mathbf{k}}_1' \hat{\mathbf{O}} \hat{\mathbf{k}}_2' = \hat{\mathbf{A}}$, $\hat{\mathbf{k}}_1'' \hat{\mathbf{U}}_{T,N} \hat{\mathbf{k}}_2'' = \hat{\mathbf{A}}$. Since $\hat{\mathbf{A}}$ is diagonal in the Bell basis, $\hat{\mathbf{k}}_1', \hat{\mathbf{k}}_2', \hat{\mathbf{k}}_1'', \hat{\mathbf{k}}_2''$ are obtained by diagonalization, and their combination yields $\hat{\mathbf{k}}_1, \hat{\mathbf{k}}_2$. We first determine the local operations $\hat{\mathbf{k}}_1', \hat{\mathbf{k}}_2'$ that transform $\hat{\mathbf{U}}_{T,N}$ into the canonical form $\hat{\mathbf{A}}$. This is achieved by calculating the $g_i(\hat{\mathbf{U}}_{T,N})$ which yield the c_i and thus $\hat{\mathbf{A}}$. In the Bell basis, $\hat{\mathbf{A}}$ is diagonal and $\hat{\mathbf{k}}_1'$ and $\hat{\mathbf{k}}_2'$ are the transformations that diagonalize $\hat{\mathbf{U}}_{T,N} \hat{\mathbf{U}}_{T,N}^T$ and $\hat{\mathbf{U}}_{T,N}^T \hat{\mathbf{U}}_{T,N}$, each yielding $\hat{\mathbf{A}}^2$. Care must be taken to assure the same ordering of eigenvectors when determining $\hat{\mathbf{k}}_1'$ and $\hat{\mathbf{k}}_2'$. Repeating the same procedure for the local operations $\hat{\mathbf{k}}_1'', \hat{\mathbf{k}}_2''$ that transform the target operation $\hat{\mathbf{O}}$ into the canonical form $\hat{\mathbf{A}}$,

and combining $\hat{\mathbf{k}}_1', \hat{\mathbf{k}}_2', \hat{\mathbf{k}}_1'', \hat{\mathbf{k}}_2''$ yields $\hat{\mathbf{k}}_1, \hat{\mathbf{k}}_2$. Assuming the errors associated with the local operations $\hat{\mathbf{k}}_1, \hat{\mathbf{k}}_2$ to be small compared to the error of the non-local operation, the actual gate error, $\mathcal{E}$, is then obtained by evaluating J_T^D for $\hat{\mathbf{k}}_1 \hat{\mathbf{U}}_{T,N} \hat{\mathbf{k}}_2$,

$$\mathcal{E} = 1 - \frac{1}{N} \mathfrak{Re} \left[\text{Tr} \left\{ \hat{\mathbf{O}}^+ \hat{\mathbf{k}}_1 \hat{\mathbf{U}}_{T,N} \hat{\mathbf{k}}_2 \right\} \right] .$$

III. APPLICATIONS

We apply the local invariants optimization functional to two examples, an effective spin-spin model that can be realized by trapped polar molecules and a Rydberg gate for trapped atoms. In the first example, the Hamiltonian may become complex, making it impossible to determine *a priori* which two-qubit gates it can implement. The Hamiltonian of the second example can realize diagonal two-qubit gates only. The complexity that necessitates use of optimal control theory in this case draws from coupling the logical basis to external degrees of freedom.

A. Two-qubit gates for an effective spin-spin model

Trapped polar molecules with $^2\Sigma_{1/2}$ electronic ground states, subject to near-resonant microwave driving inducing strong dipole-dipole coupling, give rise to the effective Hamiltonian

$$\hat{\mathbf{H}}_{eff}(t) = \frac{\hbar|\Omega(t)|}{8} \sum_{i,j=1}^{4} \hat{\boldsymbol{\sigma}}_i A_{ij}(x_0, t) \hat{\boldsymbol{\sigma}}_j \qquad (15)$$

within second-order perturbation theory in the field [4] ($\hat{\boldsymbol{\sigma}}_4 = \mathbb{1}$). The couplings $A_{ij}(x_0, t) = |\Omega(t)| a_{ij}(x_0)$ depend on the distance x_0 between the molecules and on the polarization, detuning and possibly time-dependent envelope of the microwave field. We consider here SrF molecules in an optical lattice with a lattice spacing of 300 nm and microwave radiation of about 15 GHz. The qubit is represented by the spin of the valence electron of the molecule in its rotational ground state, as described in Ref. [4]. We seek to implement two-qubit gates that are locally equivalent to the B gate [15] and to CNOT, cf. Fig. 1 and Table I. The B gate allows for generating a generic two-qubit operation from just two successive applications. Arbitrary two-qubit operations can thus be implemented with a minimal count of two-qubit and single-qubit gates [15].

For a single microwave field, it is straightforward to use the methods of Section II D to determine which non-local equivalence classes are accessible under time evolution with (15). However, multiple fields are employed, as proposed in Ref. [4], to allow generation of a broad range of effective spin-spin Hamiltonians. Whenever the spin-spin interactions deriving from different fields do not commute, it becomes a non-trivial task to determine which two-qubit gates may be efficiently generated by time evolution under the combined effective Hamiltonians. Optimization of the non-local content of the quantum gate reached by time evolution then provides a useful route to find the acccessible two-qubit gates, an important task for quantum simulations with these effective spin-spin Hamiltonians. We illustrate this with an example of determining which gates are accessible under irradiation by two microwave fields with different polarizations. When one field is pulsed and the other in continuous wave (cw) modality, the effective Hamiltonian is of the form

$$\hat{\mathbf{H}}(t) = \hat{\mathbf{H}}_0 + S(t)\hat{\mathbf{H}}_1 , \qquad (16)$$

where $\hat{\mathbf{H}}_0$ and $\hat{\mathbf{H}}_1$ do not commute, and $S(t)$ denotes the envelope (shape) of the pulsed field, $0 \leq S(t) \leq 1$. We choose the polarizations to be $\alpha_0^0 = 1/\sqrt{2}$, $\alpha_+^0 = 1/\sqrt{2}$, and $\alpha_-^0 = 0$ for the cw field and $\alpha_0^1 = 0$, $\alpha_\pm^1 = 1/\sqrt{2}$ for the pulsed field. We will first optimize for the CNOT gate. For this case we assume a rotational transition detuning of 1.2 kHz and a Rabi frequency of 590 kHz for the cw field and a pulse detuning of 50 kHz. Then the drift Hamiltonian, in MHz, in the logical basis becomes

$$\hat{\mathbf{H}}_0 = \begin{pmatrix} 5.711 & 0.324 & 0.324 & 0 \\ 0.324 & -1.840 & 1.054 & 0 \\ 0.324 & 1.054 & 1.840 & 0 \\ 0 & 0 & 0 & -2.030 \end{pmatrix}, \qquad (17)$$

and the control Hamiltonian, in MHz, is given by

$$\hat{\mathbf{H}}_1 = S(t) \begin{pmatrix} -153.65 & 0 & 0 & 3.906 \\ 0 & 153.65 & 16.085 & 0 \\ 0 & 16.085 & 153.65 & 0 \\ 3.906 & 0 & 0 & -153.65 \end{pmatrix}. \qquad (18)$$
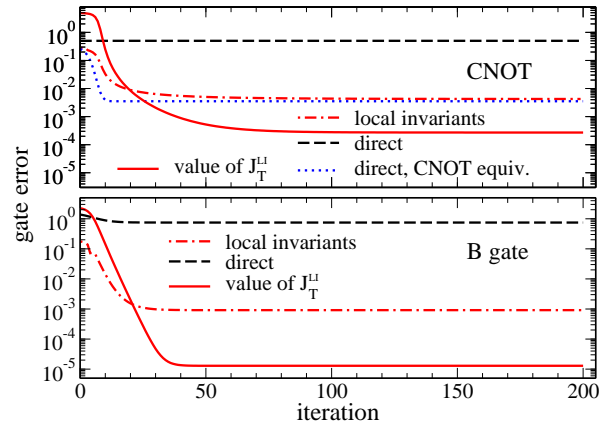

FIG. 2: (Color online) Gate error vs iteration step for direct (black dashed lines) and local invariant (red dashed-dotted lines) optimization of the CNOT and B gates with time evolution generated by Eq. (16). The blue dotted line shows the gate error for direct optimization of a specific instance of the local equivalence class [CNOT] (see text). Red solid curves display the value of the local invariants functional J_T^{LI} (for the direct optimizations the gate error is equal to the value of the functional).

The peak Rabi frequency of the pulse is 1.81 MHz. We will then optimize for the B gate. In this case the polarizations and therefore the structure of the Hamiltonian matrix are the same but the numerical values are slightly changed since we take different field parameters. Specifically, for the cw field we take the rotational transition detuning and Rabi frequency to be 1.2 kHz and 4.74 MHz, respectively, and for the pulse field we take detuning and peak Rabi frequency values of 84 kHz and 1.81 MHz, respectively. Figure 2 shows that direct optimization for CNOT and B gates is not successful, failing to find any high quality solution after a large number of iterations (dashed black lines). Thus with the structure deriving from this combination of microwave fields and polarizations, the Hamiltonian cannot generate the unitary transformations corresponding to the B gate and CNOT. In fact, it is not evident which gates from which equivalence classes can be realized from simply inspecting the Hamiltonian.

In contrast to this lack of success with direct optimization, local invariant optimization of $J = J_T^{LI} + g_a$ can be successfully used to find the time-dependent envelope $S(t)$ such that the microwave fields implement gates that are locally equivalent to the B gate [15] and to CNOT. The errors for the J_T^{LI} optimized gates are shown as a function of iteration number in Fig. 2 and compared with the results of direct optimization. Progress of optimization in the Weyl chamber is illustrated also in Fig. 1. The errors for the J_T^{LI} optimized gates in Fig. 2 are seen to be of order 10^{-3} (red dashed-dotted line). The result of standard direct optimization using J_T^D is in stark contrast to this, essentially failing to find a solution, as evidenced by the gate error remaining of order unity after 200 iter-

ations (dashed black lines). This dramatic difference reflects the fact that the Hamiltonian $\hat{\mathbf{H}}_{eff}$, when realized for the field combination of Eq. (16), cannot generate an evolution that directly yields either CNOT or B gates. However, the successful local invariant optimization *can* subsequently be used as input for a direct optimization of CNOT, as follows. Inspecting the solution for the local equivalence class [CNOT] that is obtained from optimizing J_T^{LI} shows that in this case the optimal unitary transformation is a sum of $\hat{\mathbf{U}}_d = -\frac{1}{\sqrt{2}}\,\mathsf{diag}(1-i, 1+i, 1+i, 1-i)$, which is also in [CNOT] and a smaller $\hat{\mathbf{U}}_{od}$ with all matrix elements except U_{23}, U_{32} zero. This provides motivation to specify $\hat{\mathbf{U}}_d$ as a target for direct optimization using J_T^D. We find that this leads to a solution of similar quality as using J_T^{LI} (dotted blue versus dot-dashed red line in Fig. 2). In contrast, the optimization of the local equivalence class [B] does not appear to result in an analogous dominant unitary within its equivalence class. Thus it is not possible to "guess" which representative of [B] might be implemented directly. This example illustrates how

optimization of the locally invariant functional can be used to determine what gate operations are achievable, given a possibly intricate Hamiltonian.

B. Rydberg gate with trapped neutral atoms

An application to time evolution occurring in a Hilbert space much larger than that of the quantum register is given by qubits encoded in ^{87}Rb atoms trapped by optical tweezers [16]. A non-local gate is implemented by simultaneous excitation to a Rydberg state using a near-resonant two-photon transition [5].

In the experiment of Ref. [16], the qubit states are taken to be $|0\rangle = |5s_{1/2}, F = 2, M_F = 2\rangle$, $|1\rangle = |5s_{1/2}, F = 1, M_F = 1\rangle$, the Rydberg state $|r\rangle = |58d_{3/2}, F = 3, M_F = 3\rangle$, and the intermediate state for the two-photon transition $|i\rangle = |5p_{1/2}, F = 2, M_F = 2\rangle$. In the rotating-wave approximation, the Hamiltonian for a single trapped atom reads

$$\hat{\mathbf{H}}_j^{(1)}(t) = |0\rangle\langle0| \otimes \left(\hat{\mathbf{T}} + V_{trap}(\hat{\mathbf{x}}_j)\right) + |1\rangle\langle1| \otimes \left(\hat{\mathbf{T}} + V_{trap}(\hat{\mathbf{x}}_j)\right) + |i\rangle\langle i| \otimes \left(\hat{\mathbf{T}} + \frac{\delta_R}{2}\right) + |r\rangle\langle r| \otimes \left(\hat{\mathbf{T}} + \frac{\delta_B}{2}\right)$$
$$+ \frac{\Omega_R(t)}{2}\left(|0\rangle\langle i| + |i\rangle\langle0|\right) \otimes \mathbb{1}_{\hat{\mathbf{x}}_j} + \frac{\Omega_B(t)}{2}\left(|i\rangle\langle r| + |r\rangle\langle i|\right) \otimes \mathbb{1}_{\hat{\mathbf{x}}_j}. \tag{19}$$

Here, $\hat{\mathbf{x}}_j$ denotes the position operator of atom j, $\hat{\mathbf{T}}$ the kinetic energy operator, and $\Omega_i(t)$ the time-dependent Rabi frequencies of the red and blue lasers ($\omega_R = 795$ nm and $\omega_B = 474$ nm, respectively). The maximum Rabi frequencies are taken to be $\Omega_{i,0} = 2\pi \cdot 260$ MHz, i.e., $\Omega_{R,0}$ is equal to and $\Omega_{B,0}$ larger by a factor of 10 than those of [16]. $\Omega_i(t)$ is parametrized as

$$\Omega_i(t) = \Omega_{i,0}(\tanh\varepsilon_i(t) + 1)/2 \in [0, \Omega_{i,0}],$$

with $\varepsilon_i(t)$ determined by optimal control. The detuning δ_R of the red laser is chosen to be $\delta_R = 2\pi \cdot 600$ MHz, slightly larger than in [16]. The two-photon detuning from the Rydberg level is given in terms of the Stark shift, $\delta_B = (\Omega_{B,0}^2 - \Omega_{R,0}^2)/(4\delta_R) = 0$.

The total two-atom Hamiltonian includes the long-range interaction when both atoms are in the Rydberg state,

$$\hat{\mathbf{H}}^{(2)}(t) = \hat{\mathbf{H}}_1^{(1)}(t) \otimes \mathbb{1}_{4,2} \otimes \mathbb{1}_{\hat{\mathbf{x}}_2} + \mathbb{1}_{4,1} \otimes \hat{\mathbf{H}}_2^{(1)}(t) \otimes \mathbb{1}_{\hat{\mathbf{x}}_1}$$
$$+ |rr\rangle\langle rr| \otimes \frac{u_0}{\hat{\mathbf{r}}^3}, \tag{20}$$

with $\hat{\mathbf{r}} = |\hat{\mathbf{x}}_1 - \hat{\mathbf{x}}_2|$ the inter-atomic distance. u_0 is chosen to reproduce the estimated interaction energy of 50 MHz at $r_0 = 4\,\mu$m ($u_0 = 3.284 \cdot 10^6\,\mathrm{E}_h\mathrm{a}_0^3$). With this interaction, the atoms need to spend a minimum of 10 ns in $|rr\rangle$

to pick up a non-local phase of π. In all other internal states, the interaction between the atoms at a separation of $4\,\mu$m is negligible. We approximate the optical tweezers trap by harmonic potentials and integrate over the center-of-mass motion. The trap of width, $\sigma = 0.75\,\mu$m, and depth, $V_{\min} = -4.5\,k_B$ mK, is slightly stronger than in Ref. [16].

The Hamiltonian, $\hat{\mathbf{H}}^{(2)}(t)$, is represented on an equidistant Fourier grid extending for $\pm 0.3\,\mu$m around r_0. In order to evaluate Eq. (14), the Schrödinger equation is solved simultaneously for initial states $|ij\rangle \cdot \varphi_0(r)$ ($i, j = 0, 1$) with $\varphi_0(r)$ the ground state of the trap, using a Chebychev propagator.

The errors from the optimal gates are shown in Figure 3 as a function of the corresponding optimal gate duration T and illustrate several key results. First, the large error resulting from direct optimization of CNOT (blue triangles) shows that $\hat{\mathbf{H}}^{(2)}(t)$ cannot generate CNOT directly. Second, the minimum errors of the Rydberg gate are comparable for optimization with J_T^D and J_T^{LI} (with a slight advantage for the functional based on the local invariants [21]) and both of these values reflect the quantum speed limit [17]. Third, if spontaneous emission from $|i\rangle$ is neglected (filled symbols), the minimum gate duration of ~ 40 ns to achieve high fidelities is determined primarily by the interaction strength in the Rydberg state.
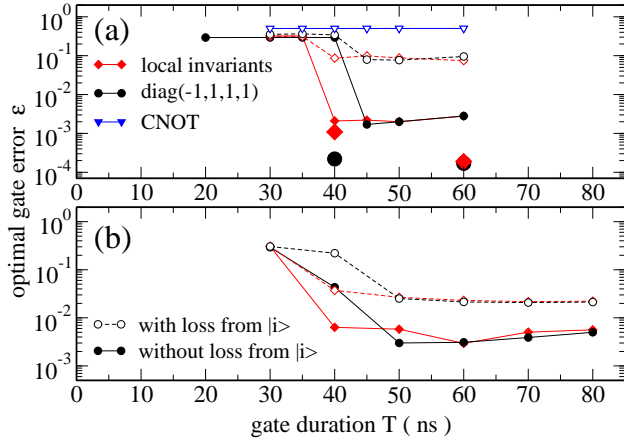
FIG. 3: (Color online) Optimal gate error as a function of the gate duration for Rydberg gate optimization based on local equivalence classes (J_T^{LI}) and on direct optimization (J_T^D) of two specific two-qubit gates (π-phase $\equiv$ diag$(-1, 1, 1, 1)$ and CNOT) without (a) and with (b) an additional constraint suppressing population in the intermediate state $|i\rangle = |5p_{1/2}\rangle$. Dashed lines with open symbols (solid lines with filled symbols): simulation including (neglecting) spontaneous emission from $|i\rangle$. Large filled symbols: calculations with trapping potential kept on during the gate.
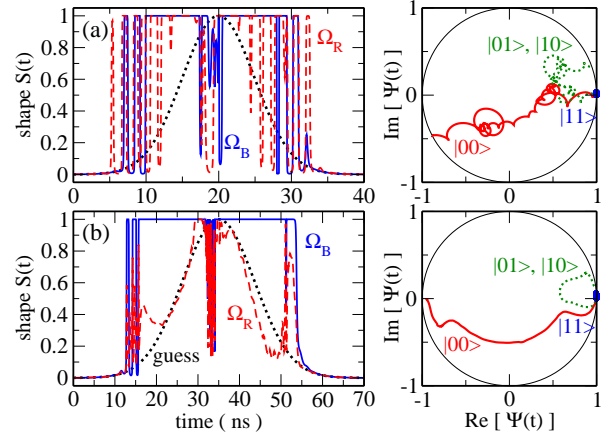

FIG. 4: (Color online) Left: optimal Rabi frequencies without (a) and with (b) spontaneous emission from $|i\rangle$. Black dotted line represents the initial "guess" pulse form. Right: corresponding dynamics of the two-qubit basis states in the complex plane.

Motion of the atoms in the trap leads to larger minimum gate errors for increasing gate duration. Gate errors close to the fault tolerance threshold of 10^{-4} are obtained only when the trapping potential is kept on during the gate (large filled symbols in Fig. 3(a)).

The main limiting factor for a high-fidelity implementation of the Rydberg gate using this particular near-resonant two-photon transition is due to spontaneous emission from the intermediate state $|i\rangle$ as is evident from Fig. 3 (open symbols). Imposing an additional constraint suppressing population of $|i\rangle$, cf. Eq. (3), leads to improved solutions but leaves the minimum errors still two orders of magnitude above the fault tolerant threshold (Fig. 3(b)). Near resonant intermediate states should therefore be avoided by suitable choice of Rydberg and intermediate states, for given laser frequencies.

Sample Rabi frequencies for optimized pulses and the corresponding two-qubit state dynamics are shown in Fig. 4. Without spontaneous emission, the minimum gate duration for which a high-fidelity implementation of CNOT can be obtained is 40 ns. The optimal pulses consist of a sequence of fast switches pumping population in a ladder-like fashion. This is reflected by the small circles of $|01\rangle$, $|10\rangle$ states in the complex plane, indicating clearly non-adiabatic dynamics. The time between switches corresponds to the duration of a π-pulse at the maximally allowed Rabi frequencies $\Omega_{i,0}$. Correspondingly, the spectra (not shown) consist of modulated sidebands spaced by $\Omega_{i,0}$. Experimentally, switches of the field amplitude on a nanosecond timescale can be generated using standard electronics (electro- or acousto-optical modulators). When spontaneous emission from the intermediate state

is taken into account in the optimization using the additional constraint g_b, the smallest gate errors achievable for the given detunings and maximum Rabi frequencies are of a few percent. This requires gate durations of 50 ns or more, which is *larger* than the gate durations without spontaneous emission. While surprising at first glance, it reflects the fact that the only way to avoid populating $|i\rangle$ is by adiabatic passage, and adiabaticity requires sufficient time. Correspondingly, the optimal Rabi frequencies in Fig. 4(b) show a double STIRAP-like behavior [18]: In the first half of the time interval, the blue pulse connecting $|i\rangle$ and $|r\rangle$ takes the role of the Stokes laser and precedes the red pulse connecting $|0\rangle$ and $|i\rangle$ which corresponds to the pump laser. In the second half of the time interval, these roles are reversed. The optimal entangling strategies in the two examples are thus based on well-known, robust and feasible control schemes – population transfer to and from the Rydberg state via π-pulses or STIRAP. The additional twist that is afforded by optimal control is speed-up, i.e., implementation of the shortest possible gate duration. This comes at a comparatively low price – additional modulations in the optimal fields on a nanosecond timescale translating into spectra whose bandwidth never exceeds a few GHz. It should therefore be comparatively straightforward to implement these optimal pulses in an experiment.

Both with and without spontaneous emission, the qubit phase dynamics (right panel of Fig. 4) show achievement of the desired non-local phase, $\chi = \phi_{00} - \phi_{01} - \phi_{10} + \phi_{11}$, with complete freedom in the local phases. This confirms the fact that J_T^{LI} imposes fewer constraints than direct optimization. Since spontaneous emission from intermediate states can be eliminated by suitable choice of atomic states and exciting lasers, it is evident that this non-local optimal control allows a high-fidelity implementation of the Rydberg gate to be achieved even

IV. SUMMARY AND CONCLUSIONS

By constructing a new optimization functional based on the local invariants of two-qubit operations, we have shown how to extend optimal control theory to take specific requirements of quantum information applications into account. In particular, we have developed an automated way to determine for a given physical system whether a desired non-local content can be realized, and if so which two-qubit operation in that desired local equivalence class can best be realized. We have illustrated the power of this approach with two examples relevant to quantum simulations and quantum computation. The first example addressed the time dependent control of effective spin Hamiltonians generated by trapped dipolar molecules. It showed that optimization of non-local content of two-qubit operations by local invariant optimization allows determination of which gates may be reached from complex Hamiltonians with non-commutative time dependence. The second example addressed the performance of a Rydberg gate with trapped atoms. It demonstrated that use of optimal control theory with the local invariant functional yields a faster gate than direct optimization, in the presence of both coupling between internal and external degrees of freedom and spontaneous emission.

The new optimization functional J_T^{LI} can easily be adapted to target all perfect entanglers, using the geometric definition of these derived in [3]. A related question of optimizing multi-partite entanglement was recently addressed using time-local control theory [19]. Local invariant optimization is expected to display its full potential in the presence of decoherence, particularly when distinct two-qubit gates in the same local equivalence class are differently affected by the decoherence. The required extension to open quantum systems is the subject of future work.

Acknowledgments

Appendix A: Explicit form of the local invariants functional

Using the definitions of $\hat{\mathbf{m}}$ and the local invariants, Eqs. (8) and (10), the functional is expressed in terms of the states,

$$J_T^{LI} = f_1^2 + f_2^2 + f_3^2 + f_4^2 + 1 - \frac{1}{N} \, \text{Tr} \left\{ \hat{\mathbf{U}}_{T,N} \hat{\mathbf{U}}_{T,N}^{+} \right\}$$

with

$$
\begin{aligned}
f_1 &= \Re \left[a_0 \det \left\{ \hat{\mathbf{U}}_{T,N} \right\} \right] - \frac{1}{16} \sum_{k,l} \left[\vec{\alpha}_k^2 \vec{\alpha}_l^2 + \vec{\beta}_k^2 \vec{\beta}_l^2 \right. \\
&\quad \left. - 2\vec{\alpha}_k^2 \vec{\beta}_l^2 - 4 \left(\vec{\alpha}_k \cdot \vec{\beta}_k \right) \left(\vec{\alpha}_l \cdot \vec{\beta}_l \right) \right] \\
f_2 &= \Im \left[a_0 \det \left\{ \hat{\mathbf{U}}_{T,N} \right\} \right] - \frac{1}{16} \sum_{k,l} \left[4\vec{\alpha}_k^2 \left(\vec{\alpha}_l \cdot \vec{\beta}_l \right) \right. \\
&\quad \left. - 4\vec{\beta}_k^2 \left(\vec{\alpha}_l \cdot \vec{\beta}_l \right) \right] \\
f_3 &= \Re \left[b_0 \det \left\{ \hat{\mathbf{U}}_{T,N} \right\} \right] - \frac{1}{4} \sum_{k,l} \left[\vec{\alpha}_k^2 \vec{\alpha}_l^2 + \vec{\beta}_k^2 \vec{\beta}_l^2 - 2\vec{\alpha}_k^2 \vec{\beta}_l^2 \right. \\
&\quad - 4 \left(\vec{\alpha}_k \cdot \vec{\beta}_k \right) \left(\vec{\alpha}_l \cdot \vec{\beta}_l \right) - \left(\vec{\alpha}_k \cdot \vec{\alpha}_l \right)^2 - \left(\vec{\beta}_k \cdot \vec{\beta}_l \right)^2 \\
&\quad \left. + 2 \left(\vec{\alpha}_k \cdot \vec{\alpha}_l \right) \left(\vec{\beta}_k \cdot \vec{\beta}_l \right) + 4 \left(\vec{\alpha}_k \cdot \vec{\alpha}_l \right) \left(\vec{\beta}_k \cdot \vec{\beta}_l \right) \right] \\
f_4 &= \Im \left[b_0 \det \left\{ \hat{\mathbf{U}}_{T,N} \right\} \right] - \frac{1}{4} \sum_{k,l} \left[4\vec{\alpha}_k^2 \left(\vec{\alpha}_l \cdot \vec{\beta}_l \right) \right. \\
&\quad - 4\vec{\beta}_k^2 \left(\vec{\alpha}_l \cdot \vec{\beta}_l \right) - 4 \left(\vec{\alpha}_k \cdot \vec{\alpha}_l \right) \left(\vec{\alpha}_k \cdot \vec{\beta}_l \right) \\
&\quad \left. + 4 \left(\vec{\beta}_k \cdot \vec{\beta}_l \right) \left(\vec{\alpha}_k \cdot \vec{\beta}_l \right) \right],
\end{aligned}
$$

where the sum runs over the N logical basis states. The constants a_0, b_0 are obtained by calculating $\hat{\mathbf{m}}$, cf. Eq. (8), for the target gate $\hat{\mathbf{O}}$,

$$
\begin{aligned}
a_0 &= \frac{\text{Tr}^2 \left\{ \hat{\mathbf{m}}_O \right\}}{16 \det\{\hat{\mathbf{O}}\}} \\
b_0 &= \frac{\left[\text{Tr}^2 \left\{ \hat{\mathbf{m}}_O \right\} - \text{Tr} \left\{ \hat{\mathbf{m}}_O^2 \right\} \right]}{4 \det\{\hat{\mathbf{O}}\}},
\end{aligned}
$$

and $\vec{\alpha}_k$ ($\vec{\beta}_k$) is the vector containing all real (imaginary) parts of the expansion coefficients of the state $|\varphi_k\rangle$ with respect to an orthonormal basis, $\{|m\rangle\}$, spanning the complete Hilbert space,

$$
\begin{aligned}
(\alpha_k)_m &= \Re \left[\langle m | \varphi_k(t) \rangle \right], \ m = 1, \ldots, \dim(\mathcal{H}) \\
(\beta_k)_m &= \Im \left[\langle m | \varphi_k(t) \rangle \right], \ m = 1, \ldots, \dim(\mathcal{H}).
\end{aligned}
$$

Note that J_T^{LI} is a polynomial of 8th degree in the states.

Appendix B: Outline of the optimization algorithm

The algorithm is determined by the functional J_T, additional time-dependent constraints g_a, g_b and the equa-

tions of motion [12] and given by the following set of equations:

1. Forward propagation to obtain the new states $|\varphi_k^{(i+1)}(t)\rangle$,

$$\frac{d}{dt}|\varphi_k^{(i+1)}(t)\rangle = -\frac{i}{\hbar}\hat{\mathbf{H}}[\epsilon^{(i+1)}]|\varphi_k^{(i+1)}(t)\rangle\,. \qquad \text{(B1)}$$

The initial states are given by the basis expansion of the time evolution operator, i.e., the logical basis states in our case.

2. Backward propagation to obtain the adjoint states $|\chi_k^{(i)}(t)\rangle$, containing an inhomogeneity if $g_b \neq 0$,

$$\frac{d}{dt}|\chi_k^{(i)}(t)\rangle = -\frac{i}{\hbar}\hat{\mathbf{H}}[\epsilon^{(i)}]|\chi_k^{(i)}(t)\rangle + |\eta\rangle \qquad \text{(B2)}$$

with the 'initial' condition at time $t = T$ determined by J_T,

$$|\chi_k(T)\rangle = \nabla_{\langle\varphi|}J_T\,, \qquad \text{(B3)}$$

and the inhomogeneity

$$|\eta\rangle = \nabla_{\langle\varphi|}g_b\,. \qquad \text{(B4)}$$

3. The equation to determine the new field from $|\varphi_k^{(i+1)}(t)\rangle$ and $|\chi_k^{(i)}(t)\rangle$, Eq. (14), with $\sigma(t)$ given by

$$\sigma(t) = C(T - t) - A\,. \qquad \text{(B5)}$$

The constants A and C are parameters of the algorithm that can be estimated analytically (based on a worst case scenario) or numerically [12]. For the local invariants functional, J_T^{LI}, the analytical estimate yields $A = 90$ for Hamiltonian (15) and $A = 580$ for Hamiltonian (20), while numerically $A = 5$ and $A = 20$, respectively, turned out to be sufficient. $C = 0$ for $g_b = 0$ and $C \leq -\lambda_b/NT$ for $g_b \neq 0$.

Compared to a linear version of the Krotov algorithm [2], the additional effort consists only in storing the forward propagated states from the previous iteration, $|\varphi_k^{(i)}(t)\rangle$, and calculating $|\Delta\varphi_k(t)\rangle$ and $\sigma(t)$.

[1] M. Nielsen and I. L. Chuang, *Quantum Computation and Quantum Information* (Cambridge University Press, 2000).
[2] J. P. Palao and R. Kosloff, Phys. Rev. A **68**, 062308 (2003).
[3] J. Zhang, J. Vala, S. Sastry, and K. B. Whaley, Phys. Rev. A **67**, 042313 (2003).
[4] A. Micheli, G. K. Brennen, and P. Zoller, Nature Phys. **2**, 341 (2006).
[5] D. Jaksch, J. I. Cirac, P. Zoller, S. L. Rolston, R. Côté, and M. D. Lukin, Phys. Rev. Lett. **85**, 2208 (2000).
[6] J. P. Palao, R. Kosloff, and C. P. Koch, Phys. Rev. A **77**, 063412 (2008).
[7] A. Konnov and V. Krotov, Automation and Remote Control **60**, 1427 (1999).
[8] S. E. Sklarz and D. J. Tannor, Phys. Rev. A **66**, 053619 (2002).
[9] W. Zhu, J. Botina, and H. Rabitz, J. Chem. Phys. **108**, 1953 (1998).
[10] Y. Maday and G. Turinici, J. Chem. Phys. **118**, 8191 (2003).
[11] M. H. Goerz, T. Calarco, and C. P. Koch, J. Phys. B **44**, 150411 (2011), special issue on quantum control theory for coherence and information dynamics.
[12] D. M. Reich, M. Ndong, and C. P. Koch, 1008.5126.
[13] S. Helgason, *Differential geometry, Lie groups, and symmetric spaces* (Academic, New York, 1978).
[14] Y. Makhlin, Quant. Inf. Proc. **1**, 243 (2002).
[15] J. Zhang, J. Vala, S. Sastry, and B. Whaley, Phys. Rev. Lett. **93**, 020502 (2004).
[16] A. Gaëtan, Y. Miroshnychenko, T. Wilk, A. Chotia, M. Viteau, D. Comparat, P. Pillet, A. Browaeys, and P. Grangier, Nature Phys. **5**, 115 (2009).
[17] T. Caneva, M. Murphy, T. Calarco, R. Fazio, S. Montangero, V. Giovannetti, and G. E. Santoro, Phys. Rev. Lett. **103**, 240501 (2009).
[18] K. Bergmann, H. Theuer, and B. W. Shore, Rev. Mod. Phys. **70**, 1003 (1998).
[19] F. Platzer, F. Mintert, and A. Buchleitner, Phys. Rev. Lett. **105**, 020501 (2010).
[20] λ_a and λ_b are numerical parameters of the algorithm: The choice of λ_a determines the magnitude of the change in the field, i.e., the step size, and thus convergence speed [2]. The ratio of λ_a and λ_b controls the relative weight of the two constraints. If $\lambda_b \ll \lambda_a$, g_b plays only a minor role, if $\lambda_b \gg \lambda_a$, g_b is strictly enforced. The latter typically comes at the expense of slower convergence since optimization under an additional constraint represents a more difficult control problem [6].
[21] For local-invariants optimization the gate duration needs to be augmented by the duration of the additional one-qubit operations before and after the non-local gate. However the one-qubit operations are at least one order of magnitude faster than the non-local gates.